Hindawi
Wireless Communications and Mobile Computing
Volume 2017, Article ID 9207108, 16 pages
https://doi.org/10.1155/2017/9207108

Research Article

Efficient Offline Waveform Design Using Quincunx/Hexagonal Time-Frequency Lattices

Raouia Ayadi,[1] Inès Kammoun,[2] and Mohamed Siala[1]

[1]*MEDIATRON Laboratory, Sup'Com, University of Carthage, 2083 Ariana, Tunisia*
[2]*LETI Laboratory, ENIS, 3038 Sfax, Tunisia*

Correspondence should be addressed to Raouia Ayadi; raouia.ayadi@supcom.tn

Received 29 June 2017; Revised 16 October 2017; Accepted 5 November 2017; Published 26 November 2017

Academic Editor: Milos Tesanovic

Conventional orthogonal frequency division multiplexing (OFDM) may turn to be inappropriate for future wireless cellular systems services, because of extreme natural and artificial impairments they are expected to generate. Natural impairments result from higher Doppler and delay spreads, while artificial impairments result from multisource transmissions and synchronization relaxation for closed-loop signaling overhead reduction. These severe impairments induce a dramatic loss in orthogonality between subcarriers and OFDM symbols and lead to a strong increase in intercarrier interference (ICI) and intersymbol interference (ISI). To fight against these impairments, we propose here an optimization of the transmit/receive waveforms for filter-bank multicarrier (FBMC) systems, with hexagonal time-frequency (TF) lattices, operating over severe doubly dispersive channels. For this, we exploit the Ping-pong Optimized Pulse Shaping (POPS) paradigm, recently applied to rectangular TF lattices, to design waveforms maximizing the signal-to-interference-plus-noise ratio (SINR) for hexagonal TF lattices. We show that FBMC, with hexagonal lattices, offers a strong improvement in SINR with respect to conventional OFDM and an improvement of around 1 dB with respect to POPS-FBMC, with rectangular lattices. Furthermore, we show that hexagonal POPS-FBMC brings more robustness to frequency synchronization errors and offers a 10 dB reduction in out-of-band (OOB) emissions, with respect to rectangular POPS-FBMC.

1. Introduction

OFDM is now a well-established technique that provides high-data-rate wireless communications through a transformation of the frequency-selective channel into several nonselective subchannels, thereby reducing the ISI [1]. For all standardized systems, OFDM uses a rectangular waveform, in order to ensure maximum spectral efficiency, while maintaining orthogonality between the different shifts of the used waveform in the TF plane. Unfortunately, in practice, the mobile radio channel is highly TF dispersive, causing an orthogonality loss between the TF shifted versions of this rectangular waveform. By adding a cyclic prefix (CP), the conventional OFDM system becomes less sensitive to delay spread and time synchronization errors, at the cost of a spectrum efficiency loss. However, in the presence of Doppler spread and frequency synchronization errors, the bad frequency localization of the rectangular waveform leads to a very important ICI, in both downlink and uplink channels. Moreover, at the uplink channel, guard bands between users accessing the spectrum resources are required because of the misalignment nature of multiple access and the strong out-of-band (OOB) power leakages between adjacent user bands, leading to an inefficient use of spectrum resources.

With respect to LTE-A, future wireless cellular systems are expected to support new applications and services, such as Tactile Internet, the Internet of things (IoT), and machine type communications (MTC) [2–4]. In order to reduce latency and efficiently use energy and radio spectrum resources for all these applications and services, it is necessary to alleviate the synchronization mechanism overhead for sporadic and small packet transmissions. Here, synchronization alleviation means the reduction of the signaling load by tolerating large synchronization errors. Unfortunately, decreasing signaling by synchronization alleviation or relaxation introduces artificial impairments, caused by timing and carrier frequency offset shifts. In addition, other extra artificial impairments, caused by delay spread and multisource

transmissions, such as a CoMP, MBMS, and cloud-radio access networks (C-RAN), are expected to be prevalent. These delay and frequency spreads cannot be tolerated and endured by conventional OFDM, leading to either a dramatic loss in spectral efficiency or a strong decrease in SINR. To face all these impairments, a plethora of research activities have focused on waveform design. Waveform design is precisely the concern for this paper, which proposes a new technique to optimize the transmit/receive waveforms.

1.1. Related Works on Waveform Design. Waveform design dates back to the work of Le Floch et al. in [5] and Haas and Belfiore [6] in 1995. In [5], a transformation of the Gaussian waveform into an orthogonal waveform with slightly worse localization was proposed as the so-called Isotropic Orthogonal Transform Algorithm (IOTA) approach. In [6], the most localized Hermite functions including the Gaussian waveform were combined in order to obtain a partially orthogonal and well TF-localized waveform. Since then, the problem of waveform optimization has been extensively investigated. The first series of research works focused on continuous-time waveform optimization. In [7], the authors proposed a method for orthogonalizing the Gaussian waveform and introduced an optimization of the TF lattices for TF dispersive channels, in order to minimize ICI/ISI. They concluded that the use of hexagonal lattices outperforms the use of rectangular ones. However, the continuous-time proposed waveforms are orthogonalized but not well TF-localized [8], leading to lower robustness to TF dispersive channels. This motivated some subsequent research works to abandon the strict orthogonality for the modulated waveforms and to focus on the good localization of these waveforms in TF plane. In [9], the authors have derived a TF well-localized continuous-time waveform for hexagonal lattices, by minimizing the mean power of ISI and ICI. However, they overlooked the mean power of the useful signal leading to a reduction in SIR. In the aforementioned works, the same waveform is considered at transmission and reception sides. To give an additional degree of freedom in waveform design, some research works proposed to consider different waveforms at transmission and reception. In [10], the authors presented two methods for optimal continuous-time design of the transmit and receive waveforms of BFDM systems over dispersive channels based on ISI/ICI-minimizing. Stojanovic et al. derived, in [11], TF well-localized waveforms for BFDM systems based on a quasi-Newton method with line search for the minimization of the interference power. In [12], based on SINR maximization, we proposed a novel approach to design continuous-time nonorthogonal well-localized transmit/receive waveforms for rectangular lattices. The proposed waveforms, which are expressed as linear combinations of the most TF-localized Hermite waveforms, demonstrated an extra robustness to doubly dispersive channels. The main drawbacks behind continuous-time optimization are significant optimization complexity and performance degradation following discretization, subsequently required in the system implementation stage. Accordingly, in more than one respect, a single-step discrete-time waveform design is more advantageous than a two-step continuous-time design. The discrete-time design is, therefore, an active area of research for either OFDM or filter-bank multicarrier (FBMC) systems. Although the theory of FBMC has a long history close to OFDM [13], it has recently been considered as a promising waveform for 5G systems, to enhance spectral efficiency with respect to the conventional CP-OFDM thanks to CP-less transmission and guard-band reduction [14]. In [15], Siala et al. optimized the discrete-time nonorthogonal waveforms, for rectangular lattices, operating over doubly dispersive channels. For this, they exploit the POPS paradigm based on SINR maximization. In [16], the authors proposed an optimization design of QAM-FBMC waveform that provides superior spectrum confinement and higher spectral efficiency compared to conventional OFDM. Furthermore, recent research projects, such as PHYDYAS [17] and 5GNOW [4], thoroughly studied FBMC in the 5G applications framework. They also considered some other waveforms suitable for 5G applications, such as generalized frequency division multiplexing (GFDM) [18] and universal filtered multicarrier (UFMC) [19]. These projects proposed off-the-shelf waveforms obtained empirically in order to reduce secondary lobes and therefore to decrease OOB emissions. These waveforms meet the requirements for which they have been designed, with no guarantee for the provision of good SINR over strongly dispersive channels.

1.2. Work Motivation and Contributions of the Paper. This paper is concerned with the optimization of FBMC waveforms for hexagonal TF lattices, accounting for both natural and artificial impairments, expected in future wireless applications and services. The first objective of the paper is to specify an iterative method for waveform optimization for hexagonal lattices, using the POPS paradigm introduced in [15] for rectangular lattices and further investigated in [20]. The second objective is to assess whether the use of hexagonal lattices, instead of rectangular lattices, actually brings a noteworthy improvement in performance, as claimed in [7, 9], or not. Our main contributions can be outlined as follows:

(i) We present a general mathematical framework for waveform optimization for hexagonal lattices and detail the approach for SINR computation. We stress the fact that the analytical derivation of the SINR is not straightforward and different from that for rectangular lattices [15].

(ii) We evaluate the gain, in terms of SINR, brought by hexagonal lattices compared to rectangular ones. Moreover, we determine through numerical results the situations for which the hexagonal lattices outperform the rectangular lattices.

(iii) We compare, through numerical results, the OOB emission of hexagonal and rectangular lattices, with optimized waveforms, and conventional OFDM. It is worth noting here that OOB is not included as a criterion in waveform optimization although it can be in practice, since OOB could be expressed as a quadratic form of the transmitted waveform.

(iv) We characterize the robustness of POPS-FBMC with respect to frequency and time synchronization and channel spread factor estimation errors. We also compare the robustness of the optimized systems on hexagonal and rectangular lattices to that of conventional OFDM.

With respect to existing works, the proposed approach provides five main advantages:

(i) It is based on SINR maximization instead of partial ICI/ISI minimization, as performed in [9].

(ii) It considers the exact optimization in the discrete-time domain with a finite waveform support instead of continuous-time optimization with an infinite waveform support, followed by discretization and truncation in time [9] that can lead to a performance degradation. Thus, the resulting waveforms can be directly implementable in hardware.

(iii) The strategy adopted in this paper for waveform optimization offers more simplicity and accuracy than the optimization method proposed in [12].

(iv) Our work can be implemented for any frequency band and discrete-time channel that satisfies the Wide-Sense Stationary Uncorrelated Scattering (WSSUS) criterion.

(v) Performed offline, the proposed iterative optimization strategy can be carried out for a finite bunch of representative propagation channel dispersion statistics, for all expected novel services (such as CoMP, MBMS, and C-RAN). The resulting optimized transmit/receive waveform pairs form a codebook and are then used online, in an adaptive fashion, to better adapt to the slowly varying channel propagation statistics. More specifically, as in adaptive modulation and coding (AMC), adaptive waveform communications (AWC) could become a reality in future wireless communications, whereby the most suitable pair of transmit-receive waveforms is selected from the codebook and used, as a function of an estimate of the current channel dispersion statistics.

1.3. Organization of This Paper. The rest of this paper is organized as follows. In Section 2, we introduce the system model. We analyse the interference and noise statistical characteristics in Section 3. In Section 4, we present the optimization procedure of the transmit/receive waveforms, based on SINR maximization. Then, in Section 5, we detail the approach for signal and interference Kernels computation. Finally, we devote Section 6 to simulation results and Section 7 to concluding this paper.

1.4. Notations. Throughout the paper, the norm of a vector is denoted by $\|\cdot\|$ and the Hermitian scalar product of two vectors is represented by $\langle\cdot,\cdot\rangle$. The operators $(\cdot)^T$, $(\cdot)^*$, $(\cdot)^H$, and $\mathbb{E}(\cdot)$ stand for transposition, complex conjugation, transconjugation, and expectation, respectively. We denote by $\otimes$ the Kronecker matrix product and by $\odot$ the component-wise product (also known as the Hadamard matrix product). The notations $(\cdot)_q$ and $(\cdot)_{pq}$ are used to refer to vector and components matrix entries generically indexed by q and (p,q), respectively. The function $[\mathbf{W},\mathbf{\Lambda}] = \text{eig}(\mathbf{A})$ produces a diagonal matrix $\mathbf{\Lambda}$ of eigenvalues and a matrix $\mathbf{W}$ whose columns are the corresponding eigenvectors of matrix $\mathbf{A}$, while the function $[\mathbf{w},\lambda] = \text{eigs}(\mathbf{A})$ returns the eigenvector $\mathbf{w}$ associated with the maximum eigenvalue λ of matrix $\mathbf{A}$. Finally, $\mathbf{I}_m$ represents the $m \times m$ identity matrix and $J_0(\cdot)$ denotes the 0th-order Bessel function of the first kind.

2. System Model

2.1. Transmitter and Receiver Models. We consider a baseband model of a multicarrier system with Q subcarriers, regularly spaced by F in frequency. The transmitted multicarrier signal is sampled at a sampling rate $R_s = 1/T_s$, where $T_s = T/N$ is the sampling period, T is the OFDM symbol period, and N is an integer accounting for the number of samples per OFDM symbol period. Due to the hexagonal nature of the TF lattices and the underlying half-symbol period shift between consecutive subcarriers, N must be even, leading to a slight flexibility reduction with respect to the rectangular TF lattices, where N could also be odd. The subcarrier spacing, F, is related to the sampling period and to the number of subcarriers by $1/F = QT_s$. In this study, the TF lattice density, $\Delta = 1/FT$, is taken below unity, leading to undersampled TF lattices in the Weyl-Heisenberg frame theory jargon. The undersampled nature of the lattices, acquired by taking Q smaller than N, offers flexibility and room to absorb and put up with different impairments inflicted by the channel and the transmitter and receiver imperfections. It is also to be noted that the positive difference $(N - Q)T_s$ is equivalent to the notion of guard interval time in conventional OFDM.

Working in the discrete-time domain at both transmitter and receiver, the sampled version of the transmitted signal is represented by the infinite vector

$$\mathbf{e} = \left(\ldots, e_{-2}, e_{-1}, e_0, e_1, e_2, \ldots\right)^T = \left(e_q\right)_{q\in\mathbb{Z}}^T, \tag{1}$$

where e_q is the transmitted signal sample at time qT_s, with $q \in \mathbb{Z}$. This vector can be written as

$$\mathbf{e} = \sum_{m,n} a_{mn}\boldsymbol{\varphi}_{mn}, \tag{2}$$

where the function $\boldsymbol{\varphi}_{mn}$, used for the transmission of symbol a_{mn}, results from a time shift, by t_{mn}, and a frequency shift, by f_{mn}, of the transmit waveform vector $\boldsymbol{\varphi}$, and a_{mn}, $m, n \in \mathbb{Z}$, are independent identically distributed modulated symbols, of zero mean and common mean transmit energy $E_s = \mathbb{E}[|a_{mn}|^2]\|\boldsymbol{\varphi}\|^2$. As illustrated in Figure 1, the TF shifts, dictated by quincunx/hexagonal lattices, are determined by the generator matrix [7, 9]

$$\begin{pmatrix} t_{mn} \\ f_{mn} \end{pmatrix} = \begin{pmatrix} T & \frac{T}{2} \\ 0 & F \end{pmatrix} \begin{pmatrix} n \\ m \end{pmatrix}. \tag{3}$$

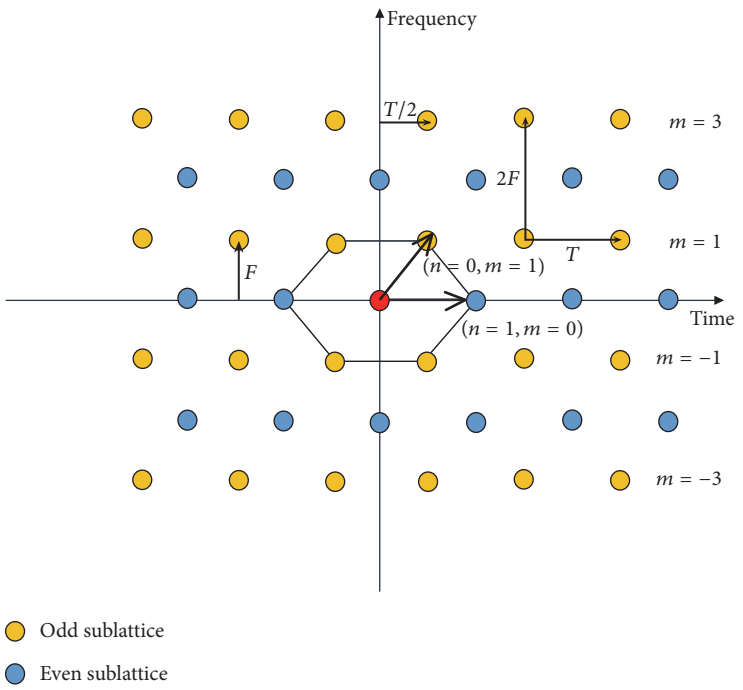

Figure 1: A hexagonal lattice in the TF plane.

Consequently, the shifted waveforms are defined by

$$\boldsymbol{\varphi}_{mn} = \boldsymbol{\sigma}_{(n+m/2)N}\left(\boldsymbol{\varphi}\right) \odot \left(e^{j2\pi mq/Q}\right)_q, \tag{4}$$

where $\boldsymbol{\sigma}_k(\boldsymbol{\varphi})$ is obtained by shifting $\boldsymbol{\varphi}$ by k samples, corresponding to a time shift by kT_s. In order to reduce the optimization complexity and the latency, the transmit waveform is assumed to have a finite duration, $D_{\boldsymbol{\varphi}}$, and thus a finite number of samples, $N_{\boldsymbol{\varphi}} = D_{\boldsymbol{\varphi}}/T_s$, where $N_{\boldsymbol{\varphi}}$ is a positive integer.

By considering a time-varying channel, the sampled version of the received signal, $\mathbf{r} = (r_q)_{q\in\mathbb{Z}}$, is determined by

$$r_q = \sum_p h\left(p,q\right) e_{q-p} + n_q = \sum_{mn} a_{mn}\left(\widetilde{\boldsymbol{\varphi}}_{mn}\right)_q + n_q, \tag{5}$$

where $(\widetilde{\boldsymbol{\varphi}}_{mn})_q = \sum_p h(p,q)(\boldsymbol{\varphi}_{mn})_{q-p}$ is the qth sample of the channel-distorted version, $\widetilde{\boldsymbol{\varphi}}_{mn}$, of $\boldsymbol{\varphi}_{mn}$, $h(p,q)$ is the impulse response of the discrete channel at time qT_s, and n_q is a discrete-time complex additive white Gaussian noise (AWGN), the samples of which are centered and uncorrelated, with common variance N_0.

The decision variable on the transmitted symbol a_{mn} is obtained by

$$\Lambda_{mn} = \langle \boldsymbol{\psi}_{mn}, \mathbf{r}\rangle = \boldsymbol{\psi}_{mn}^H \mathbf{r}, \tag{6}$$

where $\boldsymbol{\psi}_{mn}$ is a TF shifted version of the receive waveform, $\boldsymbol{\psi}$, defined by

$$\boldsymbol{\psi}_{mn} = \boldsymbol{\sigma}_{(n+m/2)N}\left(\boldsymbol{\psi}\right) \odot \left(e^{j2\pi mq/Q}\right)_q. \tag{7}$$

Likewise, the receive waveform is assumed to have a finite duration, $D_{\boldsymbol{\psi}}$, and thus a finite number of samples, $N_{\boldsymbol{\psi}} = D_{\boldsymbol{\psi}}/T_s$, which is taken as a positive integer. In order to better adapt to the possible discrepancy in the complexity capabilities of both transmitter and receiver, we can consider different durations of the transmit and receive waveforms.

2.2. Channel Model. The discrete-time channel is assumed to satisfy the WSSUS criterion, with discrete autocorrelation function [21]

$$\begin{aligned}\phi_h\left(p_1,p_2;\Delta q\right) &= E\left[h^*\left(p_1;q\right)h\left(p_2;q+\Delta q\right)\right]\\ &= \phi_h\left(p_1;\Delta q\right)\delta\left(p_2-p_1\right),\end{aligned} \tag{8}$$

where $\delta(\cdot)$ is the Kronecker delta, $\phi_h(p) = \phi_h(p;0)$ is the channel multipath-power profile, and

$$S\left(p,\nu\right) = \sum_{\Delta q}\phi_h\left(p,\Delta q\right)e^{-2j\pi\nu T_s\Delta q} \tag{9}$$

is the channel scattering function. For a simplified derivation of the expression of the SINR, to be maximized as a function of the transmit and receive waveforms, we start by considering a channel with a finite number, K, of paths, with channel impulse response

$$h\left(p,q\right) = \sum_{k=0}^{K-1} h_k \exp\left(j2\pi\nu_k T_s q\right)\delta\left(p-p_k\right), \tag{10}$$

where h_k, ν_k, and p_k are, respectively, the amplitude, the Doppler frequency shift, and the normalized time delay

shift of the kth path, with a time delay $p_k T_s$. The paths amplitudes, h_k, are assumed to be centered and decorrelated random complex Gaussian variables with average powers $\pi_k = \mathbb{E}[|h_k|^2]$. The channel scattering function is therefore given by

$$S(p,\nu) = \sum_{k=0}^{K-1} \pi_k \delta(p - p_k)\, \delta(\nu - \nu_k). \tag{11}$$

In reality, this function corresponds to a two-dimensional convolution between the scattering function and the joint probability distribution of synchronization errors in time and frequency.

Without any loss of generality, we assume the channel to be of normalized average power, meaning that $\sum_{k=0}^{K-1} \pi_k = 1$, in order to maintain the same average energy per symbol at the transmission and reception sides.

3. Analysis of Average Useful, Interference, and Noise Powers

For simplicity sake, and without loss of generality, we focus on the reception of symbol a_{00}. While referring to (6), Λ_{00} is expressed as

$$\begin{aligned}\Lambda_{00} &= \left\langle \boldsymbol{\psi}_{00}, \sum_{mn} a_{mn} \widetilde{\boldsymbol{\varphi}}_{mn} \right\rangle + \langle \boldsymbol{\psi}_{00}, \mathbf{n} \rangle \\ &= a_{00} \langle \boldsymbol{\psi}_{00}, \widetilde{\boldsymbol{\varphi}}_{00} \rangle + \sum_{(m,n)\neq(0,0)} a_{mn} \langle \boldsymbol{\psi}_{00}, \widetilde{\boldsymbol{\varphi}}_{mn} \rangle \\ &\quad + \langle \boldsymbol{\psi}_{00}, \mathbf{n} \rangle,\end{aligned} \tag{12}$$

where $\mathbf{n} = (n_q)_{q\in\mathbb{Z}}$ is the received noise vector. We note that the decision variable Λ_{00} is composed of a desired term and interference and noise terms. Based on this expression of the decision variable, we can define the useful signal power as

$$\begin{aligned}P_S &= \frac{E_s}{\|\boldsymbol{\varphi}\|^2} \mathbb{E}\left[\left| \langle \boldsymbol{\psi}_{00}, \widetilde{\boldsymbol{\varphi}}_{00} \rangle \right|^2 \right] \\ &= \frac{E_s}{\|\boldsymbol{\varphi}\|^2} \boldsymbol{\psi}_{00}^H \mathbb{E}\left[\widetilde{\boldsymbol{\varphi}}_{00} \widetilde{\boldsymbol{\varphi}}_{00}^H \right] \boldsymbol{\psi}_{00} = \frac{E_s}{\|\boldsymbol{\varphi}\|^2} \boldsymbol{\psi}^H \mathbf{KS}_{S(p,\nu)}^{\boldsymbol{\varphi}} \boldsymbol{\psi},\end{aligned} \tag{13}$$

with $\mathbf{KS}_{S(p,\nu)}^{\boldsymbol{\varphi}}$ being the useful Kernel matrix defined by

$$\mathbf{KS}_{S(p,\nu)}^{\boldsymbol{\varphi}} = \sum_{k=0}^{K-1} \pi_k \boldsymbol{\phi}_{\nu_k} \odot \left(\boldsymbol{\sigma}_{p_k}(\boldsymbol{\varphi})\, \boldsymbol{\sigma}_{p_k}(\boldsymbol{\varphi})^H \right), \tag{14}$$

where $\boldsymbol{\phi}_{\nu_k}$ is the Hermitian matrix with (p,q)th entry $e^{2j\pi T_s \nu_k (p-q)}$. Similarly, by considering the decorrelated and centered nature of the transmitted symbols, we can write the mean power of the interference term as

$$\begin{aligned}P_I &= \frac{E_s}{\|\boldsymbol{\varphi}\|^2} \sum_{(m,n)\neq(0,0)} \mathbb{E}\left[\left| \langle \boldsymbol{\psi}_{00}, \widetilde{\boldsymbol{\varphi}}_{mn} \rangle \right|^2 \right] \\ &= \frac{E_s}{\|\boldsymbol{\varphi}\|^2} \sum_{(m,n)\neq(0,0)} \boldsymbol{\psi}_{00}^H \mathbb{E}\left[\widetilde{\boldsymbol{\varphi}}_{mn} \widetilde{\boldsymbol{\varphi}}_{mn}^H \right] \boldsymbol{\psi}_{00} \\ &= \frac{E_s}{\|\boldsymbol{\varphi}\|^2} \boldsymbol{\psi}^H \mathbf{KI}_{S(p,\nu)}^{\boldsymbol{\varphi}} \boldsymbol{\psi},\end{aligned} \tag{15}$$

where $\mathbf{KI}_{S(p,\nu)}^{\boldsymbol{\varphi}}$ is the intersymbol interference Kernel, given by

$$\begin{aligned}\mathbf{KI}_{S(p,\nu)}^{\boldsymbol{\varphi}} &= \sum_{k=0}^{K-1} \pi_k \boldsymbol{\phi}_{\nu_k} \\ &\quad \odot \sum_{(m,n)\neq(0,0)} \left(\boldsymbol{\sigma}_{p_k}(\boldsymbol{\varphi}_{mn})\, \boldsymbol{\sigma}_{p_k}(\boldsymbol{\varphi}_{mn})^H \right).\end{aligned} \tag{16}$$

Finally, the average power of the noise term is expressed as

$$P_N = \mathbb{E}\left[\left| \langle \boldsymbol{\psi}_{00}, \mathbf{n} \rangle \right|^2 \right] = \boldsymbol{\psi}_{00}^H \mathbb{E}\left[\mathbf{n}\mathbf{n}^H \right] \boldsymbol{\psi}_{00} = N_0 \|\boldsymbol{\psi}\|^2. \tag{17}$$

We note that both Kernel matrices, $\mathbf{KS}_{S(p,\nu)}^{\boldsymbol{\varphi}}$ and $\mathbf{KI}_{S(p,\nu)}^{\boldsymbol{\varphi}}$, are Hermitian positive-definite. To derive the POPS optimization algorithm, to be presented in Section 4, we also note that these Kernels obey the equalities

$$\begin{aligned}\boldsymbol{\psi}^H \mathbf{KS}_{S(p,\nu)}^{\boldsymbol{\varphi}} \boldsymbol{\psi} &= \boldsymbol{\varphi}^H \mathbf{KS}_{S(-p,-\nu)}^{\boldsymbol{\psi}} \boldsymbol{\varphi}, \\ \boldsymbol{\psi}^H \mathbf{KI}_{S(p,\nu)}^{\boldsymbol{\varphi}} \boldsymbol{\psi} &= \boldsymbol{\varphi}^H \mathbf{KI}_{S(-p,-\nu)}^{\boldsymbol{\psi}} \boldsymbol{\varphi}.\end{aligned} \tag{18}$$

Consequently, given the receiver waveform $\boldsymbol{\psi}$, we can write the useful signal power and the mean power of the interference as quadratic functions in the transmit waveform $\boldsymbol{\varphi}$, with the new Kernels $\mathbf{KS}_{S(-p,-\nu)}^{\boldsymbol{\psi}}$ and $\mathbf{KI}_{S(-p,-\nu)}^{\boldsymbol{\psi}}$, respectively. Again, using these new Kernels, we can optimize the transmitter waveform $\boldsymbol{\varphi}$ through a maximization of the SINR.

4. Optimization Procedure

The SINR, defined as the ratio of the mean power of the useful signal, in (13), and the mean power of the interference and noise terms, in (15) and (17), respectively, is used as the optimization criterion. The maximization of this SINR leads to the optimum pair of transmit and receive waveforms

$$\left(\boldsymbol{\varphi}^{\text{opt}}, \boldsymbol{\psi}^{\text{opt}} \right) = \arg \max_{\boldsymbol{\varphi},\boldsymbol{\psi}} \text{SINR}. \tag{19}$$

To determine the couple $(\boldsymbol{\varphi}, \boldsymbol{\psi})$ that maximizes (19), we express explicitly the SINR as function of $\boldsymbol{\varphi}$ and $\boldsymbol{\psi}$ as follows:

$$\begin{aligned}\text{SINR} &= \frac{P_S}{P_I + P_N} = \frac{\boldsymbol{\psi}^H \mathbf{KS}_{S(p,\nu)}^{\boldsymbol{\varphi}} \boldsymbol{\psi}}{\boldsymbol{\psi}^H \mathbf{KI}_{S(p,\nu)}^{\boldsymbol{\varphi}} \boldsymbol{\psi} + \text{SNR}^{-1} \|\boldsymbol{\varphi}\|^2 \|\boldsymbol{\psi}\|^2} \\ &= \frac{\boldsymbol{\varphi}^H \mathbf{KS}_{S(-p,-\nu)}^{\boldsymbol{\psi}} \boldsymbol{\varphi}}{\boldsymbol{\varphi}^H \mathbf{KI}_{S(-p,-\nu)}^{\boldsymbol{\psi}} \boldsymbol{\varphi} + \text{SNR}^{-1} \|\boldsymbol{\psi}\|^2 \|\boldsymbol{\varphi}\|^2},\end{aligned} \tag{20}$$

where SNR $= E_s/N_0$ is the signal-to-noise ratio. In some favorable transmission scenarios, the noise term is negligible with respect to the interference term, resulting in a measure of the SIR, as a substitute of the SINR. Let

$$\mathbf{KIN}^{\boldsymbol{\varphi}}_{S(p,\nu)} = \mathbf{KI}^{\boldsymbol{\varphi}}_{S(p,\nu)} + \mathrm{SNR}^{-1} \left\|\boldsymbol{\varphi}\right\|^2 \mathbf{I}_{N_\psi} \tag{21}$$

be the interference plus noise Kernel used in the quadratic form of the SINR denominator. Referring to (18), the optimization problem in (19) is equivalent to a maximization of a generalized Rayleigh quotient involving an optimization of the receive waveform $\boldsymbol{\psi}$, for a given transmit waveform $\boldsymbol{\varphi}$, and an optimization of the transmit waveform $\boldsymbol{\varphi}$, for a given receive waveform $\boldsymbol{\psi}$. In many respects, our algorithm behaves like the Lloyd-Max algorithm, which is used for quantization optimization, by repeatedly finding the centroid of each set in the partition and then repartitioning the input according to which of these centroids is closest. Several algorithms can be used for an iterative offline optimization of this problem. Thanks to its proven numerical stability, the SINR optimization algorithm adopted in this paper consists in diagonalizing the denominator $\mathbf{KIN}^{\boldsymbol{\varphi}}_{S(p,\nu)}$ and making a basis change, so that the maximization amounts to finding the maximum-eigenvalue eigenvector of a quadratic form. More precisely, we first decompose the Kernel $\mathbf{KIN}^{\boldsymbol{\varphi}}_{S(p,\nu)}$ as

$$\mathbf{KIN}^{\boldsymbol{\varphi}}_{S(p,\nu)} = \mathbf{U}\boldsymbol{\Lambda}\mathbf{U}^H, \tag{22}$$

where $\mathbf{U}$ is a unitary matrix and $\boldsymbol{\Lambda}$ is a diagonal matrix with nonnegative eigenvalues corresponding to the eigenvectors of $\mathbf{KIN}^{\boldsymbol{\varphi}}_{S(p,\nu)}$. Second, we make a basis change in the Kernel $\mathbf{KIN}^{\boldsymbol{\varphi}}_{S(p,\nu)}$ as

$$\boldsymbol{\psi}^H \mathbf{KIN}^{\boldsymbol{\varphi}}_{S(p,\nu)} \boldsymbol{\psi} = \boldsymbol{\psi}^H \mathbf{U}\boldsymbol{\Lambda}\mathbf{U}^H \boldsymbol{\psi} = \mathbf{u}^H \mathbf{u}, \tag{23}$$

with the introduction of the vector $\mathbf{u} = \boldsymbol{\Lambda}^{1/2}\mathbf{U}^H\boldsymbol{\psi}$.

Banking on the fact that $\mathbf{KI}^{\boldsymbol{\varphi}}_{S(p,\nu)}$ is a positive Hermitian matrix, while referring to (21), we are sure that all eigenvalues of $\boldsymbol{\Lambda}$ are greater than or equal to SNR^{-1} and therefore are strictly positive. Hence, we can recover $\boldsymbol{\psi}$ from $\mathbf{u}$ as $\boldsymbol{\psi} = \mathbf{U}\boldsymbol{\Lambda}^{-1/2}\mathbf{u}/\|\mathbf{U}\boldsymbol{\Lambda}^{-1/2}\mathbf{u}\|$, up to a normalizing multiplicative factor, avoiding any numerical instability. By replacing this new expression of the receive waveform $\boldsymbol{\psi}$ in the expression of the SINR, we end up with

$$\mathrm{SINR} = \frac{\mathbf{u}^H \boldsymbol{\Phi} \mathbf{u}}{\mathbf{u}^H \mathbf{u}}, \tag{24}$$

with $\boldsymbol{\Phi} = \boldsymbol{\Lambda}^{-1/2}\mathbf{U}^H \mathbf{KS}^{\boldsymbol{\varphi}}_{S(p,\nu)} \mathbf{U}\boldsymbol{\Lambda}^{-1/2}$ being a positive Hermitian matrix. Consequently, the maximization of the SINR consists in finding the maximum eigenvalue of $\boldsymbol{\Phi}$ and its associated eigenvector $\mathbf{u}$. The stages of this optimization approach are detailed in Algorithm 1.

In perfect agreement with the POPS paradigm introduced in [15], Algorithm 1 is an offline iterative algorithm, composed of an initialization stage and an iterative stage. In the initialization stage, the good choice of the transmit waveform initialization is very critical in order to ensure the convergence of the algorithm to a global maximum of the SINR, which results in the best optimized transmit and receive waveforms. In each iteration k of the iterative stage, we proceed through two major steps:

(i) A first step dedicated to the optimization of the receive waveform, $\boldsymbol{\psi}^{(k)}$, given the previously obtained transmit waveform $\boldsymbol{\varphi}^{(k)}$. This step is referred to as the "ping" step.

(ii) A second step dedicated to the optimization of the transmit waveform, $\boldsymbol{\varphi}^{(k+1)}$, given the previously obtained receive waveform $\boldsymbol{\psi}^{(k)}$. This step is referred to as the "pong" step.

Accordingly, the proposed optimization approach is referred to as the POPS algorithm, since it is based on "ping" and "pong" steps, to compute, offline, the best transmit and receive waveforms for any transmission impairments.

5. Computation of Simplified Versions of Useful and Interference Kernels

The complexity of the proposed approach could be categorized with respect to offline and online processing. On the one hand, offline processing, which is the concern of the present paper, is done once and beforehand, with the aim of finding the most suitable codebook size, under a complexity-efficiency compromise perspective, the best representative statistics of the channel, and the best corresponding pairs of transmit-receive waveforms. This processing can rely on standard, general, and familiar software, such as MATLAB, and requires a very short time (several minutes) for the optimization of the whole set of codebooks required for all applications or mechanisms (such as CoMP or MBMS, C-RAN, and the random access channel). On the other hand, online processing encompasses standard waveform filtering, at both transmit and receive sides, as well as run-of-river channel statistics estimation and transmitter-receiver signaling, to adapt the transmit-receive waveform pair to the changing propagation statistics. Among these tasks, filtering is by far the most computational-resource-consuming. Hence, we believe that online processing will mostly be of similar complexity to standard and thoroughly studied FBMC systems. In order to reduce the offline complexity of Algorithm 1, we next derive simplified expressions of the useful and interference Kernels (see (14) and (16)), taking into account the channel characteristics and the quincunx/hexagonal nature of multicarrier transmission. Despite the fact that the presented paradigm can take into account the cumulative effects of asynchronism, synchronization errors, and delay and Doppler spreads, briefly, we only focus next on natural impairments, brought by the channel. For this, we consider a scattering function with decoupled diffuse Doppler spectral density in the frequency domain, $\alpha(\nu)$, obeying the Jakes model [22], and a discrete-time multipath-power profile in the time domain, $\beta(p)$, obeying the exponential truncated decaying model. Hence

$$S(p,\nu) = \alpha(\nu)\,\beta(p), \tag{25}$$

Initialization stage: At this stage, we initialize $\boldsymbol{\varphi}^{(0)}$ and introduce a precision parameter $\epsilon > 0$ and the maximum number of allowed iterations.

Iterative stage: At the kth iteration, $k = 0, 1, 2, 3, \ldots$, we successively estimate the receiver waveform $\boldsymbol{\psi}^{(k)}$ and the transmitter waveform $\boldsymbol{\varphi}^{(k+1)}$ as follows:

(1) Compute the Kernels $\mathbf{KS}_{S(p,\nu)}^{\boldsymbol{\varphi}^{(k)}}$ and $\mathbf{KI}_{S(p,\nu)}^{\boldsymbol{\varphi}^{(k)}}$

(2) $\mathbf{KIN}_{S(p,\nu)}^{\boldsymbol{\varphi}^{(k)}} = \mathbf{KI}_{S(p,\nu)}^{\boldsymbol{\varphi}^{(k)}} + \mathrm{SNR}^{-1}\|\boldsymbol{\varphi}^{(k)}\|^2\mathbf{I}_{N_{\boldsymbol{\psi}}}$

(3) $[\mathbf{U}, \boldsymbol{\Lambda}] = \mathrm{eig}(\mathbf{KIN}_{S(p,\nu)}^{\boldsymbol{\varphi}^{(k)}})$

(4) $\boldsymbol{\Phi} = \boldsymbol{\Lambda}^{-1/2}\mathbf{U}^H\mathbf{KS}_{S(p,\nu)}^{\boldsymbol{\varphi}^{(k)}}\mathbf{U}\boldsymbol{\Lambda}^{-1/2}$

(5) $[\mathbf{u}_{\max}, \lambda_{\max}] = \mathrm{eigs}(\boldsymbol{\Phi})$

(6) $\boldsymbol{\psi}^{(k)} = \dfrac{\mathbf{U}\boldsymbol{\Lambda}^{-1/2}\mathbf{u}_{\max}}{\|\mathbf{U}\boldsymbol{\Lambda}^{-1/2}\mathbf{u}_{\max}\|}$

(7) Calculate the Kernels $\mathbf{KS}_{S(-p,-\nu)}^{\boldsymbol{\psi}^{(k)}}$ and $\mathbf{KI}_{S(-p,-\nu)}^{\boldsymbol{\psi}^{(k)}}$

(8) $\mathbf{KIN}_{S(-p,-\nu)}^{\boldsymbol{\psi}^{(k)}} = \mathbf{KI}_{S(-p,-\nu)}^{\boldsymbol{\psi}^{(k)}} + \mathrm{SNR}^{-1}\|\boldsymbol{\psi}^{(k)}\|^2\mathbf{I}_{N_{\boldsymbol{\varphi}}}$

(9) $[\mathbf{V}, \boldsymbol{\Xi}] = \mathrm{eig}(\mathbf{KIN}_{S(-p,-\nu)}^{\boldsymbol{\psi}^{(k)}})$

(10) $\boldsymbol{\Gamma} = \boldsymbol{\Xi}^{-1/2}\mathbf{V}^H\mathbf{KS}_{S(-p,-\nu)}^{\boldsymbol{\psi}^{(k)}}\mathbf{V}\boldsymbol{\Xi}^{-1/2}$

(11) $[\mathbf{v}_{\max}, \vartheta_{\max}] = \mathrm{eigs}(\boldsymbol{\Gamma})$

(12) $\boldsymbol{\varphi}^{(k+1)} = \dfrac{\mathbf{V}\boldsymbol{\Xi}^{-1/2}\mathbf{v}_{\max}}{\|\mathbf{V}\boldsymbol{\Xi}^{-1/2}\mathbf{v}_{\max}\|}$

Stop condition: $\|\langle\boldsymbol{\varphi}^{(k+1)}, \boldsymbol{\varphi}^{(k)}\rangle\|/\|\boldsymbol{\varphi}^{(k+1)}\|\|\boldsymbol{\varphi}^{(k)}\| > 1 - \epsilon$ and $\|\langle\boldsymbol{\psi}^{(k+1)}, \boldsymbol{\psi}^{(k)}\rangle\|/\|\boldsymbol{\psi}^{(k+1)}\|\|\boldsymbol{\psi}^{(k)}\| > 1 - \epsilon$ or the maximum number of allowed iterations is reached.

Algorithm 1: Optimization approach.

with

$$\alpha(\nu) = \begin{cases} \dfrac{1}{\pi f_D}\dfrac{1}{\sqrt{1-(\nu/f_D)^2}}, & \text{if } |\nu| < f_D, \\ 0, & \text{if } f_D \le |\nu| \le \dfrac{1}{2T_s}, \end{cases} \tag{26}$$

where f_D is the maximum Doppler frequency shift, and

$$\beta(p) = \sum_{k=0}^{K-1}\pi_k\delta(p - p_k), \tag{27}$$

with normalized power paths $\pi_k = ((1-b)/(1-b^K))b^k$, $k = 0, 1, \ldots, K-1$, with $0 < b < 1$ being the decaying factor and K being the number of contiguous paths in the channel.

For the present channel, the useful Kernel can be written as

$$\mathbf{KS}_{S(p,\nu)}^{\boldsymbol{\varphi}} = \boldsymbol{\Pi} \odot \sum_{k=0}^{K-1}\pi_k\left(\boldsymbol{\sigma}_{p_k}(\boldsymbol{\varphi})\,\boldsymbol{\sigma}_{p_k}(\boldsymbol{\varphi})^H\right), \tag{28}$$

where $\boldsymbol{\Pi}$ is the Hermitian matrix representing the time autocorrelation function of the channel, whose (p,q)th entry is given by

$$(\boldsymbol{\Pi})_{pq} = \int \alpha(\nu)\, e^{j2\pi\nu T_s(p-q)}d\nu = J_0\left(2\pi f_D T_s(p-q)\right). \tag{29}$$

As for the second interference Kernel, for hexagonal lattices, we can write

$$\mathbf{KI}_{S(p,\nu)}^{\boldsymbol{\varphi}} = {}_{\infty}\mathbf{K}_{S(p,\nu)}^{\boldsymbol{\varphi}} - \mathbf{KS}_{S(p,\nu)}^{\boldsymbol{\varphi}}, \tag{30}$$

where ${}_{\infty}\mathbf{K}_{S(p,\nu)}^{\boldsymbol{\varphi}}$ is a new "infinite" Kernel, defined by

$${}_{\infty}\mathbf{K}_{S(p,\nu)}^{\boldsymbol{\varphi}} = {}_{\infty}\mathbf{KE}_{S(p,\nu)}^{\boldsymbol{\varphi}} + {}_{\infty}\mathbf{KO}_{S(p,\nu)}^{\boldsymbol{\varphi}}, \tag{31}$$

where

$${}_{\infty}\mathbf{KE}_{S(p,\nu)}^{\boldsymbol{\varphi}} = \boldsymbol{\Omega}_{\mathrm{e}} \odot \sum_{k=0}^{K-1}\pi_k\sum_n\left(\boldsymbol{\sigma}_{p_k+nN}(\boldsymbol{\varphi}) \odot \left(\boldsymbol{\sigma}_{p_k+nN}(\boldsymbol{\varphi})\right)^H\right) \tag{32}$$

is an "even" infinite Kernel, with

$$\boldsymbol{\Omega}_{\mathrm{e}} = \boldsymbol{\Pi} \odot \left(\sum_{\delta=0}^{Q/2-1} e^{j4\pi\delta(p-q)/Q}\right)_{(p,q)\in\mathbb{Z}^2} \tag{33}$$

being a Hermitian matrix, whose (p,q)th entry is given by

$$\begin{aligned} &(\boldsymbol{\Omega}_{\mathrm{e}})_{pq} \\ &= \begin{cases} \dfrac{Q}{2}J_0\left(2\pi f_D T_s(p-q)\right), & \text{if } (p-q) \bmod \dfrac{Q}{2} = 0 \\ 0, & \text{otherwise,} \end{cases} \\ &{}_{\infty}\mathbf{KO}_{S(p,\nu)}^{\boldsymbol{\varphi}} \\ &= \boldsymbol{\Omega}_{\mathrm{o}} \\ &\quad \odot \sum_{k=0}^{K-1}\pi_k\sum_n\left(\boldsymbol{\sigma}_{p_k+(n+1/2)N}(\boldsymbol{\varphi}) \odot \left(\boldsymbol{\sigma}_{p_k+(n+1/2)N}(\boldsymbol{\varphi})\right)^H\right) \end{aligned} \tag{34}$$

is an "odd" infinite Kernel, with

$$\mathbf{\Omega}_{\mathrm{o}} = \mathbf{\Pi} \odot \left(\sum_{\delta=0}^{Q/2-1} e^{j2\pi(2\delta+1)(p-q)/Q} \right)_{(p,q)\in\mathbb{Z}^2} \tag{35}$$

being a Hermitian matrix whose (p,q)th entry is given by

$$\left(\mathbf{\Omega}_{\mathrm{o}}\right)_{pq} = \begin{cases} -\dfrac{Q}{2} J_0\left(2\pi f_D T_s (p-q)\right), & \text{if } (p-q) \bmod Q = \dfrac{Q}{2} \\ \dfrac{Q}{2} J_0\left(2\pi f_D T_s (p-q)\right), & \text{if } (p-q) \bmod Q = 0 \\ 0, & \text{otherwise.} \end{cases} \tag{36}$$

Notice that the "even" infinite Kernel accounts for the contributions of even subcarriers presenting a zero time shift with respect to the 0th subcarrier and the "odd" infinite Kernel accounts for the contributions of the odd subcarriers presenting a half-symbol-period time shift with respect to the 0th subcarrier. Also notice that the matrices $\mathbf{\Pi}$, $\mathbf{\Omega}_{\mathrm{e}}$, and $\mathbf{\Omega}_{\mathrm{o}}$ are calculated once for the whole optimization process and are kept unchanged from one iteration to another.

As illustrated in Figure 2, we next propose an easy and efficient method to simplify the numerical calculation of the previous Kernels, $\mathbf{KS}^{\boldsymbol{\varphi}}_{S(p,\nu)}$ and $\mathbf{KI}^{\boldsymbol{\varphi}}_{S(p,\nu)}$. The calculation of these Kernels is performed at the "ping" step of each iteration k for the optimization of the receive waveform $\boldsymbol{\psi}$. Likewise, following the same process as in Figure 2, the "pong" step of each iteration banks on a determination of both Kernels, $\mathbf{KS}^{\boldsymbol{\psi}}_{S(-p,-\nu)}$ and $\mathbf{KI}^{\boldsymbol{\psi}}_{S(-p,-\nu)}$, by replacing the transmit waveform $\boldsymbol{\varphi}$ by the receive waveform, $\boldsymbol{\psi}$, and considering instead the inverse in time and frequency of channel scattering function. According to Figure 2(a), we start by multiplying the transmit waveform $\boldsymbol{\varphi}$ by its Hermitian transpose $\boldsymbol{\varphi}^H$. The resulting matrix is shifted according to the multipath-power profile of the channel and then entrywise multiplied with matrix $\mathbf{\Pi}$. Subsequently, the useful Kernel $\mathbf{KS}^{\boldsymbol{\varphi}}_{S(p,\nu)}$ is obtained using a selection window, in gap with that of the transmit waveform, to take into account the causality of the channel. As shown in Figures 2(a), 2(b), and 2(c), this selection window, which is common to all involved Kernels, plays a key role in the determination of the SINR as a ratio of two quadratic forms in $\boldsymbol{\psi}$. Because of the finite durations of $\boldsymbol{\varphi}$ and $\boldsymbol{\psi}$, the relative position of the time window of $\boldsymbol{\psi}$, with respect to the time window of $\boldsymbol{\varphi}$, becomes crucial and decisive in the determination of the achievable SINR. Typically, it is optimized by moving the $\boldsymbol{\psi}$ window around the average delay incurred by the channel, in steps of the sampling period T_s, and finding the best achievable SINR.

Now, in order to compute the elementary contributions to the Kernel ${}_{\infty}\mathbf{K}^{\boldsymbol{\varphi}}_{S(p,\nu)}$, we must compute the "even" and "odd" infinite Kernels. As shown in Figure 2(b), the "even" infinite Kernel, ${}_{\infty}\mathbf{KE}^{\boldsymbol{\varphi}}_{S(p,\nu)}$, is obtained by regularly and periodically shifting the shifted matrix $\sum_{k=0}^{K-1} \pi_k (\boldsymbol{\sigma}_{p_k}(\boldsymbol{\varphi})\, \boldsymbol{\sigma}_{p_k}(\boldsymbol{\varphi})^H)$ by increments of the normalized symbol duration N and multiplying the final result with matrix $\mathbf{\Omega}_{\mathrm{e}}$. Also, as shown in Figure 2(c), the "odd" interference Kernel, ${}_{\infty}\mathbf{KO}^{\boldsymbol{\varphi}}_{S(p,\nu)}$, is obtained by regularly and periodically shifting the shifted matrix $\sum_{k=0}^{K-1} \pi_k (\boldsymbol{\sigma}_{p_k}(\boldsymbol{\varphi}) \boldsymbol{\sigma}_{p_k}(\boldsymbol{\varphi})^H)$ by integer multiples of N samples starting from an initial shift by $N/2$ samples in time and, finally, multiplying this result with matrix $\mathbf{\Omega}_{\mathrm{o}}$. The infinite Kernel is obtained by selecting the window from the optimum position after summing both "even" and "odd" infinite Kernels.

In order to determine the interference Kernel $\mathbf{KI}^{\boldsymbol{\varphi}}_{S(p,\nu)}$, we subtract the useful Kernel $\mathbf{KS}^{\boldsymbol{\varphi}}_{S(p,\nu)}$ from the infinite Kernel ${}_{\infty}\mathbf{K}^{\boldsymbol{\varphi}}_{S(p,\nu)}$. Since the transmit and receive waveforms have finite durations, only a finite number of the shifts of $\sum_{k=0}^{K-1} \pi_k (\boldsymbol{\sigma}_{p_k}(\boldsymbol{\varphi}) \boldsymbol{\sigma}_{p_k}(\boldsymbol{\varphi})^H)$ actually contribute to the full determination of the selection window needed in the determination of the SINR.

6. Numerical Results

In this section, we numerically evaluate the performance of FBMC with waveforms optimized for hexagonal lattices and operating over highly TF dispersive channels, characterized by channel scattering functions obeying (25). In a first bunch of numerical results, we fix the number of subcarriers to $Q = 128$ and the spread factor to $B_d T_m = 10^{-2}$. In a second bunch of numerical results, we vary these values to study the performance of POPS-FBMC as a function of Q and $B_d T_m$. According to past experimental characterizations of the small-scale part of the propagation channel, the maximum reported delay spread, T_m, never exceeds a few microseconds [23], while the maximum Doppler frequency, B_d, never goes above a few hundred Hertz [24] for a high mobility. As a consequence, the channel spread factor of 10^{-2} is typically one to two orders of magnitude larger that practically reported values. Camping on these large values of the channel spread not only helps us tackle a worst case situation but also takes into account other synchronization and asynchronism imperfections. In order to have the best value of the SINR, we always go through a preliminary determination of the best balance between F and T with respect to B_d and T_m, respectively, while observing a given lattice density constraint $\Delta = 1/FT$. In this determination, we do not care about the optimum initialization of the POPS algorithm and stick to the Gaussian function, as an initialization of the transmit waveform, which is also the first Hermite function, that offers the best localization on the TF plane. Moreover, for simplicity sake and without loss of generality, we choose $N_{\boldsymbol{\varphi}}$ and $N_{\boldsymbol{\psi}}$ as integer multiples of N and assume a common duration, $D = D_{\boldsymbol{\varphi}} = D_{\boldsymbol{\psi}}$, for the transmitter and receiver waveforms, although these conditions are not necessary and the general case could be treated as well. We compare the obtained numerical results to two benchmarks, with the first being conventional OFDM and the second being POPS-FBMC with rectangular lattices, with the common TF shifts being, respectively, $t_{mn} = nT$ and $f_{mn} = mF$.

6.1. SINR and SIR Performances of POPS-FBMC on Quincunx/Hexagonal Lattices. In Figure 3, we present the evolution of the SINR as a function of the number of iterations,

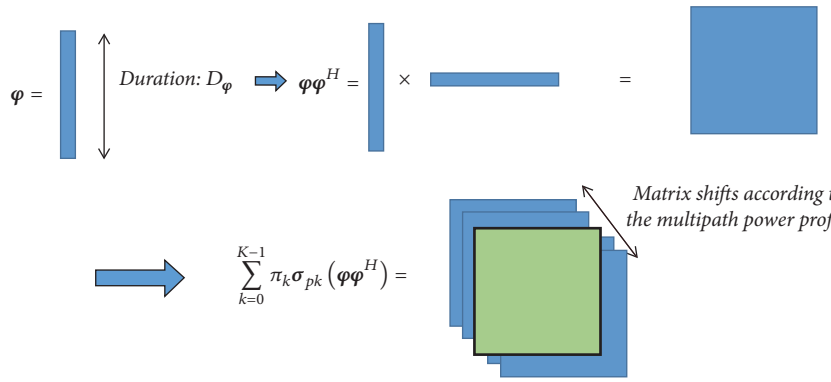

(a) Useful Kernel

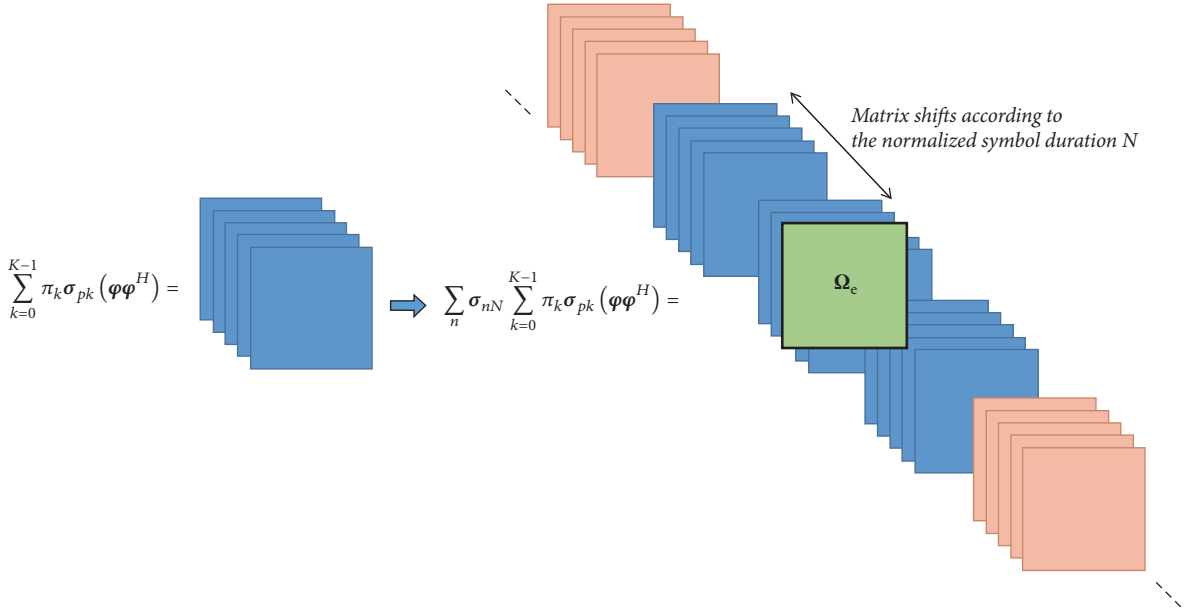

(b) "Even" infinite Kernel

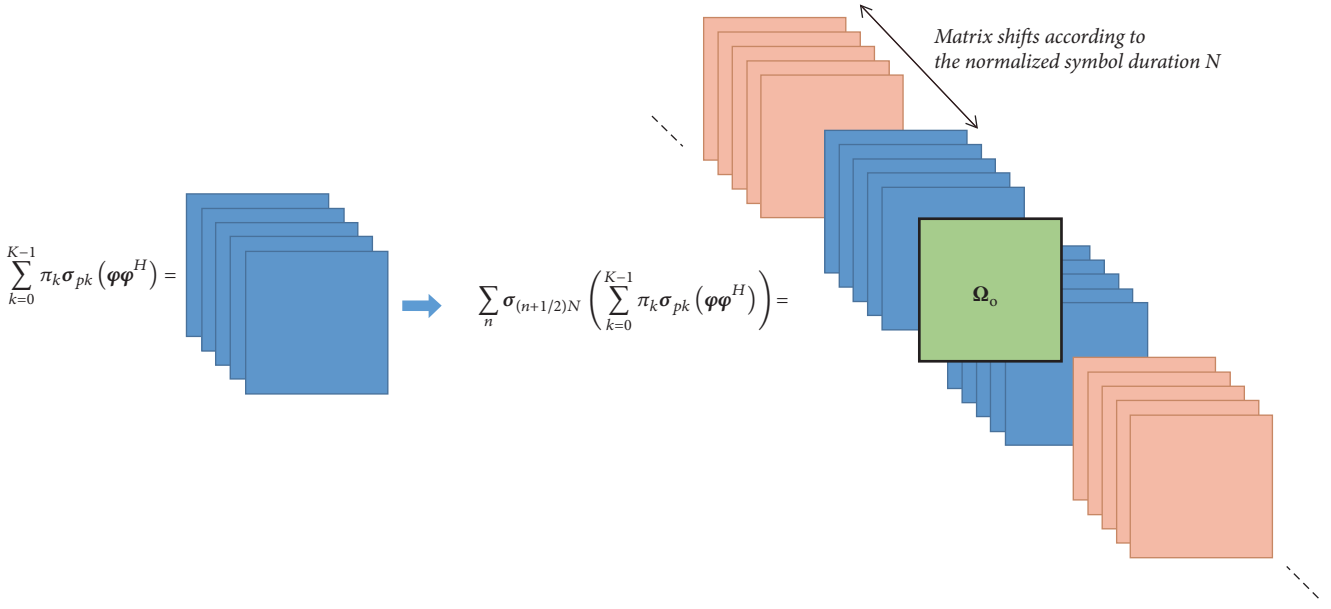

(c) "Odd" infinite Kernel

FIGURE 2: Illustration of the calculation of the useful and interference Kernels. (The pink squares of "even" and "odd" infinite Kernels do not overlap with the selection window and therefore do not contribute to the determination of the infinite Kernel.)

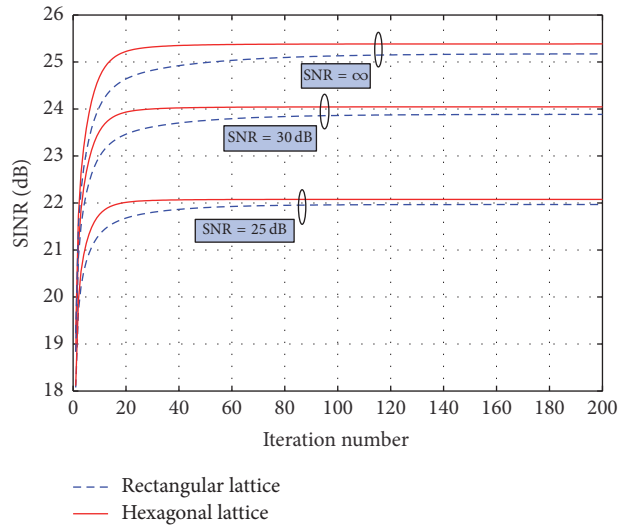

FIGURE 3: Evolution of the achievable SINR as a function of the POPS algorithm iterations, for $B_dT_m = 0.01$, $Q = 128$, CP = 32, $D = 7T$, $FT = 1.25$, and SNR = 25 dB, 30 dB, and infinity.

for hexagonal and rectangular lattices, over a TF dispersive AWGN channel, when SNR = 25 dB, 30 dB, and infinity, for a lattice density $\Delta = 1/FT = 0.8$ ($FT = 1.25$) and a waveform duration $D = 7T$. This figure shows that FBMC, with quincunx/hexagonal lattices, offers a slight improvement in SINR with respect to FBMC with rectangular lattices, for the different considered values of the SNR. We also notice the convergence of the SINR to the SNR over the a TF dispersive AWGN channel, for both rectangular and hexagonal lattices. To better illustrate this result, we draw, in Figure 4, the behavior of the optimized SINR as a function of the SNR for a hexagonal multicarrier system, for different values of the lattice density ($\Delta = 0.7, 0.8$, and 0.9) and a waveform duration $D = 7T$. This figure shows that, at low SNR, the optimized SINR is very close to the SNR value. However, at high SNR, the optimized SINR converges to the optimized SIR value obtained for a noiseless channel (i.e., $N_0 = 0$). Figure 5 shows the SIR evolution as a function of FT for optimized systems, on hexagonal and rectangular lattices, operating over TF dispersive noiseless channels. A comparison is also made with the conventional OFDM system. Different values of the waveform duration ($D = T$, $3T$, $5T$, and $7T$) are considered. Figure 5 shows an SIR enhancement for the rectangular and hexagonal multicarrier transmission systems when the waveform duration increases or the lattice density decreases. It also shows that the SIR obtained with $D = 7T$ slightly outperforms the one obtained with $D = 5T$. Figure 5 also shows that the POPS-FBMC on hexagonal lattices offers a strong improvement in SIR with respect to the conventional OFDM and a maximum improvement of 1 dB with respect to the optimized system on rectangular lattices, depending on waveform duration and lattice density. For example, when $\Delta = 0.8$ and $D = 3T$, a 5 dB (4 dB, resp.) gain is obtained with the optimized system on hexagonal (rectangular, resp.) lattices, relatively to conventional OFDM systems. Figure 6 illustrates the impact of an increase of the number of subcarriers, Q, on the SIR behavior of the optimized POPS-FBMC with hexagonal lattices. Two values of the waveform duration, $D = T$ and $D = 3T$, are considered. We observe a slight improvement in SIR when Q increases. For a further characterization of the POPS-FBMC on hexagonal lattices, we show in Figure 7 the behavior of the SIR versus the channel spread factor B_dT_m, for a lattice density $\Delta = 0.8$ and a waveform duration $D = 3T$. We also add in this figure the SIR obtained with a POPS-FBMC on rectangular lattices and a conventional OFDM. We observe a significant enhancement in SIR when the spread factor decreases for the different systems. We also note that POPS-FBMC on hexagonal lattices always outperforms POPS-OFDM on rectangular lattices and conventional OFDM, for all values of B_dT_m. More importantly, we observe that the SIR performance increases with hexagonal-lattice FBMC, with respect to the rectangular-lattice FBMC, when the channel dispersion B_dT_m increases. For example, when $B_dT_m = 10^{-2}$, a 1 dB gain is obtained with the optimized system on hexagonal lattices, relatively to the optimized system with rectangular lattices, while a 0.5 dB gain is obtained when $B_dT_m = 10^{-4}$.

6.2. Optimized Waveforms Characterization on Hexagonal Lattices. In Figure 8, we present the temporal evolution of the optimum transmit and receive waveforms corresponding to the optimized SIR, when SNR = ∞, for $\Delta = 0.9$ and $D = 7T$ and both hexagonal and rectangular lattices. For both lattices, we observe that the optimized receive waveform matches perfectly the temporal inverse of the optimized transmit waveform. Using alternative expressions of the SINR as generalized Rayleigh quotients in the receive waveform $\boldsymbol{\psi}$, we can prove that this characteristic is theoretically valid when the optimum pair of transmit/receive waveforms is unique. We also note that the main lobes of the optimized transmit and receive waveforms obtained on hexagonal lattices are more concentrated around the origin, compared to the ones on rectangular lattices. This better localization justifies the SIR performance improvement on hexagonal lattices. In Figure 9, we depict the power spectral densities (PSD) of the optimized transmit waveform for the hexagonal lattices (Figure 9(a)) as well as for 65 contiguous subcarriers (Figure 9(b)), for different waveform durations and $\Delta = 0.9$. A comparison is made with the PSD, of the conventional OFDM waveform and the POPS-optimized waveform for rectangular lattices, for $D = 7T$. First, we note that the OOB power leakage of conventional OFDM is very important, requiring an insertion of large guard bands between the subcarriers of different users, mainly at the uplink when the transmission is asynchronous and the receive power is generally unbalanced between the different communications. Second, we note that the optimized waveform on hexagonal lattices reduces the OOB emission with respect to the conventional OFDM, especially when D increases. For example, a gain of 70 dB is brought by the POPS-FBMC on hexagonal lattices with $D = 7T$, compared to the conventional OFDM system. Third, we point out a 10 dB reduction in OOB emission when we consider the hexagonal layout instead of the rectangular one. This reduction in OOB emission minimizes the interference

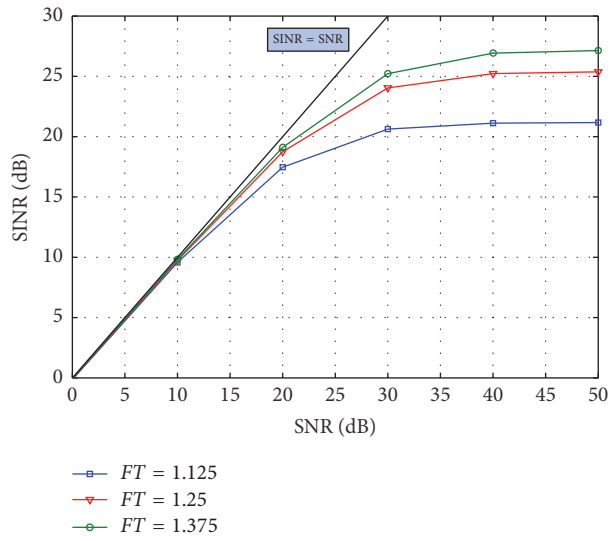

FIGURE 4: Optimized SINR versus different values of SNR, for $B_dT_m = 0.01$, $Q = 128$, and $D = 7T$.

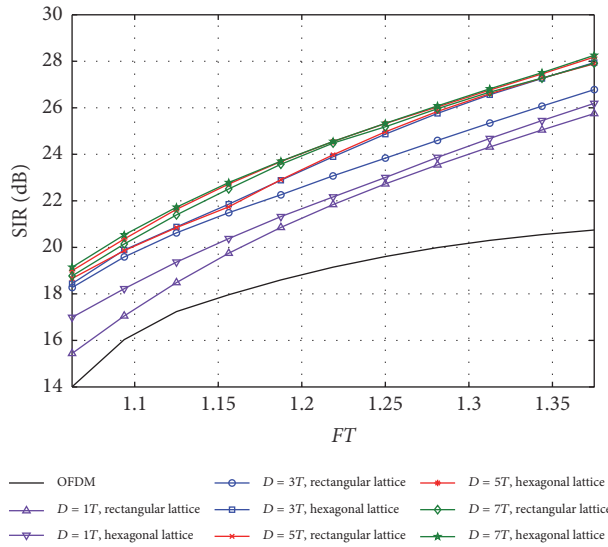

FIGURE 5: Optimized SIR versus FT, for $B_dT_m = 0.01$ and $Q = 128$.

into neighbouring bands and reduces the probability of violating spectral masks imposed by some standards.

In order to study the time-frequency localization of our optimized waveforms, we present, in Figure 10, the evolution of the Heisenberg uncertainty [25] in discrete time, ξ, as function of symbol period, T, and latency, D. This figure shows that the time-frequency localization increases linearly as a function of symbol period and latency. However, by improving latency, optimization complexity and performance in terms of SIR increase. Then, we must find a compromise between complexity, latency, and performance. This compromise makes it possible for some applications which tolerate increasing latency to benefit from an increase in SIR. For example, instead of considering a latency of T, we can use 3 or $5T$ instead to increase the SIR by 3 dB.

6.3. Robustness Characterization of POPS-FBMC on Quincunx/Hexagonal Lattices. In this subsection, we characterize the robustness of POPS-FBMC with respect to its sensitivity to frequency and time synchronization and channel spread factor estimation errors. In Figure 11(a), we compare the sensitivity to frequency synchronization errors of optimized systems on both hexagonal and rectangular lattices to that of conventional OFDM. The channel is assumed to be noiseless, meaning that SNR $= \infty$. In this figure, we consider a normalized frequency synchronization error $\Delta\nu/F$ varying between -0.1 and 0.1, a lattice density $\Delta = 0.8$, and waveform durations $D = 3T$ and $7T$. As it is expected, the SIR degrades with the increase of the frequency synchronization error. More importantly, we notice that POPS-FBMC on hexagonal lattices is less sensitive to frequency synchronization errors

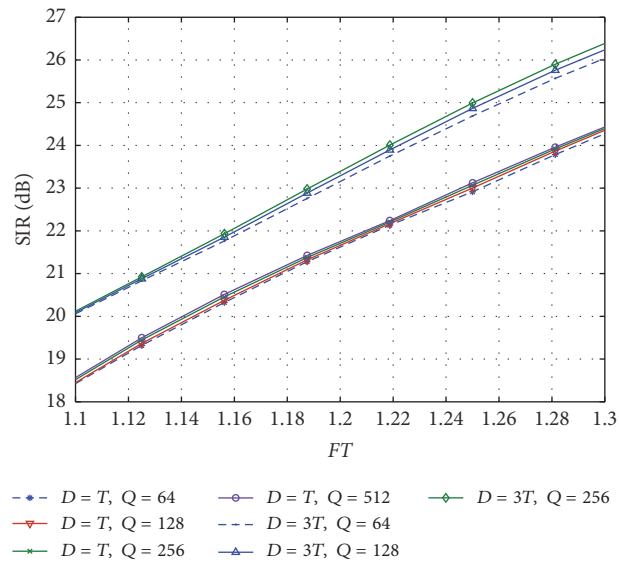

FIGURE 6: Optimized SIR versus FT, for different number of subcarriers Q, $B_dT_m = 0.01$, and $D = T$ and $3T$.

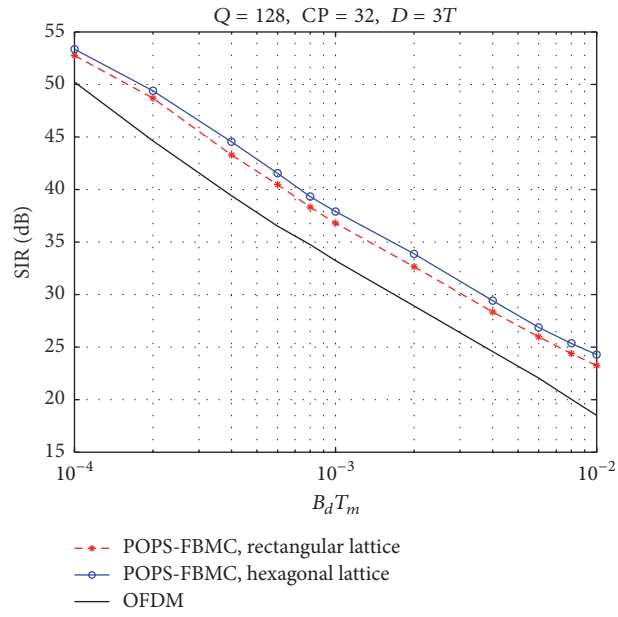

FIGURE 7: Optimized SIR as a function of the channel spread factor B_dT_m, for $Q = 128$, $FT = 1.25$, and $D = 3T$.

than POPS-FBMC on rectangular lattices. For example, a gain in terms of SIR of about 6 dB can be reached by using hexagonal-lattice waveforms instead of rectangular-lattice waveforms, for a waveform duration $D = 7T$ and $\Delta\nu/F = \pm 0.1$. Furthermore, Figure 12(b) shows the sensitivity of the optimized POPS-FBMC on hexagonal lattices to frequency synchronization errors, for different values of the lattice density ($\Delta = 0.7$, 0.8, and 0.9) and a waveform duration $D = 7T$. Notice that the hexagonal-lattice FBMC is less sensitive to frequency synchronization errors than rectangular-lattice FBMC when FT increases.

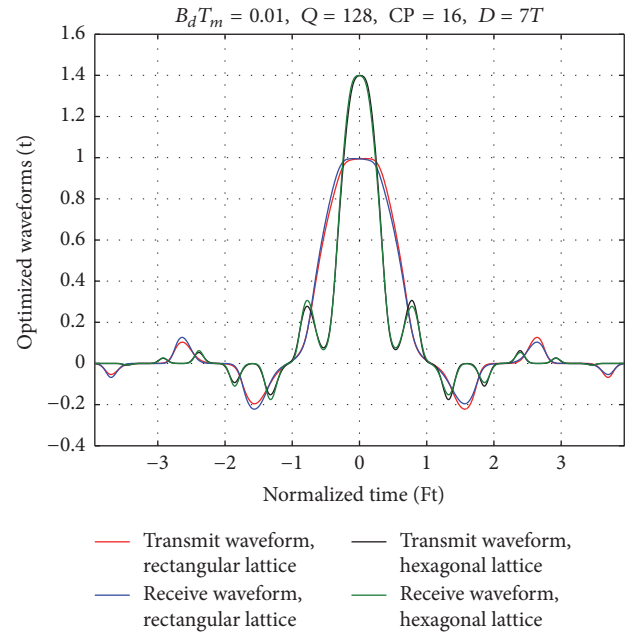

FIGURE 8: Optimized transmit and receive waveforms on the hexagonal and rectangular lattices, for $B_dT_m = 0.01$, $Q = 128$, $D = 7T$, and $FT = 1.125$.

The sensitivity of POPS-FBMC on hexagonal and rectangular lattices to time synchronization errors is shown in Figure 12(a), when the normalized time synchronization error $\Delta\tau/T_s$ varies between −40 and 40, for a lattice density $\Delta = 0.8$, waveform durations $D = 3T$ and $7T$, and a noiseless channel. Contrarily to the sensitivity to frequency synchronization errors, the POPS-FBMC with hexagonal lattices is more sensitive to ISI over a time dispersive channel than the POPS-FBMC with rectangular lattices, especially for large waveform durations. These extra sensitivity results are explained by both the narrow gap between the successive time shifts and the higher optimal value of T_m/T for hexagonal lattices as compared to rectangular ones. Nevertheless, both hexagonal and rectangular optimized systems outperform the conventional OFDM even when the time synchronization error is very important. Moreover, we show in Figure 12(b) the sensitivity to time synchronization errors of the hexagonal-lattice POPS-FBMC, for different values of FT when $D = 7T$. It is clear that POPS-FBMC with hexagonal lattices becomes less sensitive to time synchronization errors when FT increases.

Figure 13 illustrates the sensitivity of POPS-FBMC, with hexagonal lattices, to spread factor estimation errors, with actual values of B_dT_m ranging between 10^{-4} and 10^{-2}, for a lattice density $\Delta = 0.8$ and a common waveform duration $D = 3T$. We show the behavior of the achievable SIR for each of the optimal waveforms, obtained for $(B_dT_m)_1 = 10^{-4}$, $(B_dT_m)_2 = 10^{-3}$, and $(B_dT_m)_3 = 10^{-2}$, as a function of B_dT_m. In this figure, we prove the robustness of our optimized waveforms to estimation errors in B_dT_m. We observe that the SIR performance degradation, compared to the optimum case, becomes larger when the actual B_dT_m becomes smaller than the B_dT_m used for optimization of the

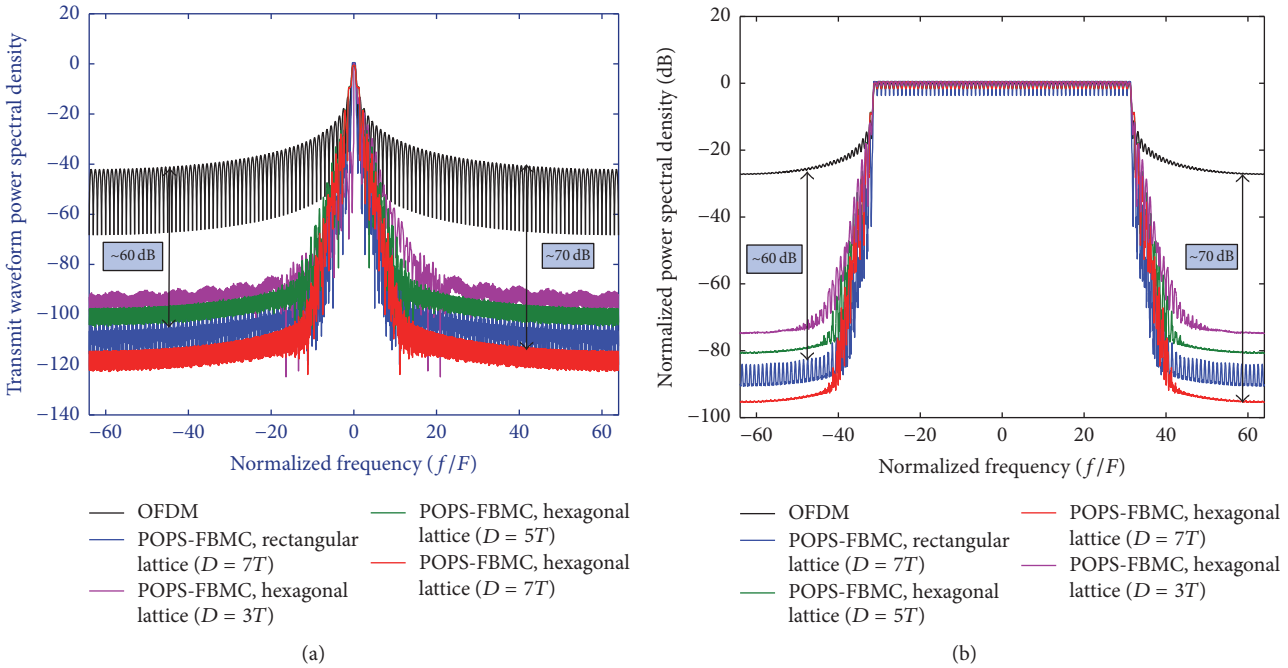

FIGURE 9: Normalized power spectral density, for $B_dT_m = 0.01$, $Q = 128$, and $FT = 1.125$. (a) One subcarrier. (b) Aggregation of 65 contiguous subcarriers.

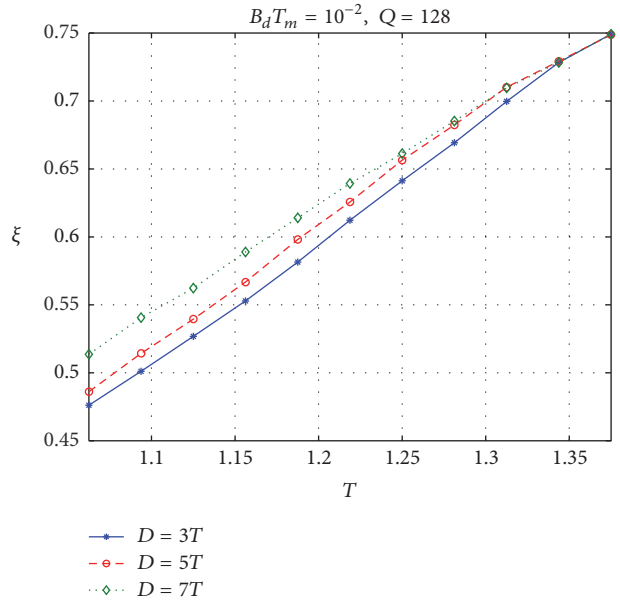

FIGURE 10: Time-frequency localization as function of symbol period, T, and latency, D, for B_dT_m and $Q = 128$.

transmit-receive waveform pair than when the actual B_dT_m becomes larger. Figure 13 is also a good illustration of how the AWC concept can be introduced in 5G systems and beyond. The idea is to determine the codebook, of required waveform pairs, suitable for an efficient adaptation of the transmit and receive waveforms to the channel statistics, while having an acceptable degradation with regard to the case of perfect knowledge of B_dT_m. More precisely, a finite number of waveform pairs could be optimized offline for several well-chosen values of B_dT_m. Then, each pair is used online, during effective transmission, for a range of values of B_dT_m around the underlying value of its optimization to outperform other pairs. As a consequence, the global obtained performance corresponds to the maximum curves of the performances of all pairs in the codebook. Compared to the ideal yet unrealistic case, where the best pair for the current value of B_dT_m is used, the performance degradation brought by the use of the codebook is conditioned by the gap between the maximum curve and the ideal curve of the SIR and the a priori statistics of the taken values of B_dT_m. Therefore, the targeted values of B_dT_m, underlying the determination of the codebook, must be well chosen to minimize the average loss in performance for a given size of the codebook.

7. Conclusion

In this paper, we proposed an optimization technique for the design of optimum transmit/receive waveforms in the discrete-time domain for FBMC systems, using hexagonal TF lattices and operating over TF dispersive channels. These waveforms are obtained by using a new approach, known as POPS, for the maximization of the SINR or the SIR at the receiver.

We have shown that the optimal SIR obtained for FBMC with hexagonal lattices outperforms the one obtained with rectangular lattices, especially for highly dispersive channels. Also, we have compared the performances of FBMC systems for both rectangular and hexagonal lattices over TF dispersive channels and demonstrated that the POPS-FBMC, with hexagonal lattices, is more efficient in the presence of

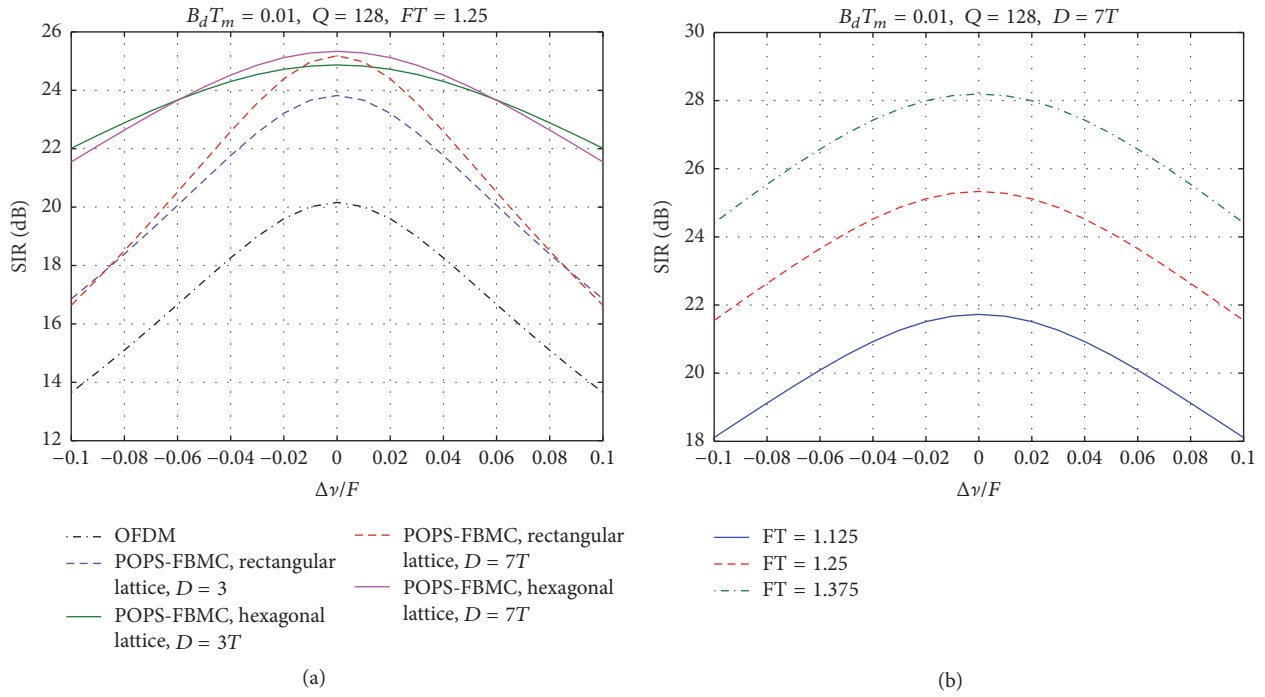

FIGURE 11: Sensitivity to synchronization errors in frequency, for $B_dT_m = 0.01$ and $Q = 128$: (a) hexagonal and rectangular lattices, $FT = 1.25$ and $D = 3T$ and $7T$; (b) hexagonal lattices and three values of FT.

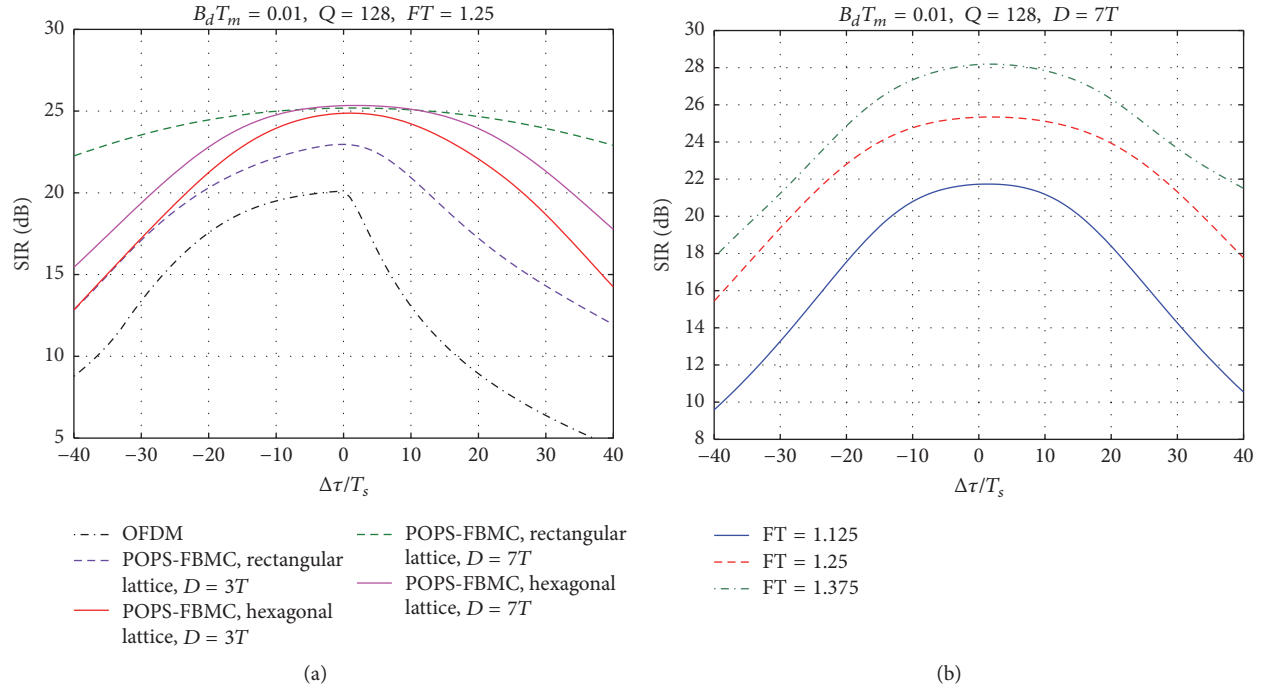

FIGURE 12: Sensitivity to synchronization errors in time, for $B_dT_m = 0.01$, $Q = 128$: (a) hexagonal and rectangular lattices, $FT = 1.25$ and $D = 3T$ and $7T$; (b) hexagonal lattices and three values of FT.

frequency synchronization errors and is more sensitive in the presence of time synchronization errors. The latter characteristic, brought in part by the hexagonal nature of the TF lattice, is not definitive and could be alleviated and even inverted, using a nonoptimal distribution of the Doppler spread and the time delay spread with respect to subcarrier frequency spacing and symbol duration. On the other hand, we have proved the dramatic increase in robustness brought by both

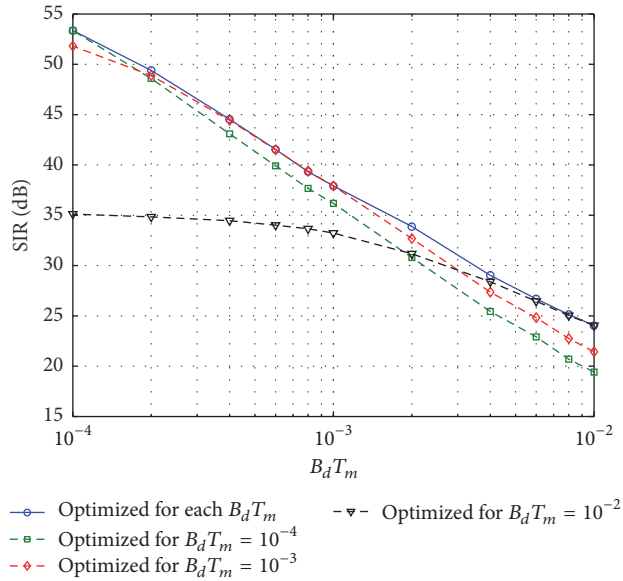

FIGURE 13: Sensitivity to an estimation error on B_dT_m, for $Q = 128$, $FT = 1.25$, and $D = 3T$.

systems relative to conventional OFDM, in the presence of TF synchronization errors. A spectral study was done and showed that the POPS-FBMC with hexagonal lattices offers a 10 dB (70 dB, resp.) reduction in OOB emissions with respect to FBMC with rectangular lattices (conventional OFDM, resp.).

In this paper, we have studied the performance of our FBMC system in terms of SINR or SIR. A study of its performance in terms of block error rate (BLER) or bit error rate (BER) will be the objective of future work. We also intend to work on multipulse waveform design [26–28] and waveform optimization for partial equalization, whereby interference from neighbouring symbols, in time or/and in frequency, is tolerated thanks to a simplified equalization at the receiver [29].

Conflicts of Interest

The authors declare that there are no conflicts of interest regarding the publication of this paper.

References

[1] B. Saltzberg, "Performance of an efficient parallel data transmission system," *IEEE Transactions on Communication Technology*, vol. 15, no. 6, pp. 805–811, 1967.

[2] G. Fettweis, "A 5G wireless communications vision," *Microwave Journal*, vol. 55, pp. 24–39, 2012.

[3] G. Wunder, M. Kasparick, S. Ten Brink et al., "5GNOW: Challenging the LTE design paradigms of orthogonality and synchronicity," in *Proceedings of the 2013 IEEE 77th Vehicular Technology Conference, VTC Spring 2013*, Germany, June 2013.

[4] G. Wunder, P. Jung, M. Kasparick et al., "5GNOW: non-orthogonal, asynchronous waveforms for future mobile applications," *IEEE Communications Magazine*, vol. 52, no. 2, pp. 97–105, 2014.

[5] B. Le Floch, M. Alard, and C. Berrou, "Coded orthogonal frequency division multiplex," *Proceedings of the IEEE*, vol. 83, no. 6, pp. 982–996, 1995.

[6] R. Haas and J. Belfiore, "Multiple carrier transmission with time-frequency well-localized impulses," *IEEE SCVT in the Benelux*, vol. 5, pp. 1–18, 1997.

[7] T. Strohmer and S. Beaver, "Optimal OFDM design for time-frequency dispersive channels," *IEEE Transactions on Communications*, vol. 51, no. 7, pp. 1111–1122, 2003.

[8] T. Strohmer, "Approximation of dual gabor frames, window decay, and wireless communications," *Applied and Computational Harmonic Analysis*, vol. 11, no. 2, pp. 243–262, 2001.

[9] F.-M. Han and X.-D. Zhang, "Hexagonal multicarrier modulation: a robust transmission scheme for time-frequency dispersive channels," *IEEE Transactions on Signal Processing*, vol. 55, no. 5, part 1, pp. 1955–1961, 2007.

[10] D. Schafhuber, G. Matz, and F. Hlawatsch, "Pulse-shaping OFDM/BFDM systems for time-varying channels: ISI/ICI analysis, optimal pulse design, and efficient implementation," in *Proceedings of the 13th IEEE International Symposium on Personal, Indoor and Mobile Radio Communications (PIMRC '02)*, vol. 3, pp. 1012–1016, IEEE, Lisbon, Portugal, September 2002.

[11] D. Stojanovic, I. Djurovic, and L. Stankovic, Biorthogonal pulses concentrated in time-frequency plane for OFDM in doubly dispersive channels, ETRAN, June 2004.

[12] R. Ayadi, I. Kammoun, and M. Siala, "Low complexity optimization and implementation of pulse shapes for BFDM systems," in *Proceedings of the 2013 IEEE 14th Workshop on Signal Processing Advances in Wireless Communications, SPAWC 2013*, pp. 699–703, Germany, June 2013.

[13] B. Farhang-Boroujeny, "OFDM versus filter bank multicarrier," *IEEE Signal Processing Magazine*, vol. 28, no. 3, pp. 92–112, 2011.

[14] F. Schaich, "Filterbank based multi carrier transmission (FBMC) - Evolving OFDM: FBMC in the context of WiMAX," in *Proceedings of the 2010 European Wireless Conference, EW 2010*, pp. 1051–1058, Italy, April 2010.

[15] M. Siala, F. Abdelkefi, and Z. Hraiech, "Novel algorithms for optimal waveforms design in multicarrier systems," in *Proceedings of the 2014 IEEE Wireless Communications and Networking Conference, WCNC 2014*, pp. 1270–1275, Turkey, April 2014.

[16] C. Kim, Y. H. Yun, K. Kim, and J.-Y. Seol, "Introduction to QAM-FBMC: from waveform optimization to system design," *IEEE Communications Magazine*, vol. 54, no. 11, pp. 66–73, 2016.

[17] M. Bellenger, "FBMC physical layer: A primer," PHYDYAS report, 2010.

[18] G. Fettweis, M. Krondorf, and S. Bittner, "GFDM—generalized frequency division multiplexing," in *Proceedings of the IEEE Vehicular Technology Conference (VTC '09)*, Barcelona, Spain, April 2009.

[19] V. Vakilian, T. Wild, F. Schaich, S. Ten Brink, and J.-F. Frigon, "Universal-filtered multi-carrier technique for wireless systems beyond LTE," in *Proceedings of the 2013 IEEE Globecom Workshops, GC Wkshps 2013*, pp. 223–228, Atlanta, Ga, USA, December 2013.

[20] Z. Hraiech, M. Siala, and F. Abdelkefi, "Numerical characterization for optimal designed waveform to multicarrier systems in 5G," in *Proceedings of the 22nd European Signal Processing Conference, EUSIPCO 2014*, pp. 156–160, September 2014.

[21] J. G. Proakis, Digital communications, ser. McGraw-Hill series in electrical and computer engineering. New York: McGraw-Hill, 1995.

[22] P. Jung and G. Wunder, "The WSSUS pulse design problem in multicarrier transmission," *IEEE Transactions on Communications*, vol. 55, no. 10, pp. 1918–1928, 2007.

[23] L. J. Greenstein and V. Erceg, "A new path-gain/delay-spread propagation model for digital cellular channels," *IEEE Transactions on Vehicular Technology*, vol. 46, no. 2, pp. 477–485, 1997.

[24] 3GPP, "Evolved universal terrestrial radio access (E-UTRA); user equipment (UE) radio transmission and reception (Release 8)," Sophia Antipolis, France, Technical specification TR 36.803, 2007.

[25] L. C. Calvez and P. Vilbe, "On the unertainty priniple in discrete signals," *IEEE Trans. On Cir. Sys.: Analog and Digital Signal Processing*, vol. 6, pp. 394-395, Jun 1992.

[26] M. M. Hartmann, G. Matz, and D. Schafhuber, "Wireless multicarrier communications via multipulse Gabor Riesz bases," *EURASIP Journal on Applied Signal Processing*, vol. 2006, 2006.

[27] Multipulse multicarrier communications over varying fading channels: performance analysis and system optimization, IEEE ICASSP, Montreal, Canada, pp. 805–808, May 2004.

[28] M. Bellili, L. B. H. Slama, and M. Siala, "Multi-pulse/single-pulse design for maximizing SIR in partially equalized OFDM systems over highly dispersive channels," in *Proceedings of the 2009 16th IEEE International Conference on Electronics, Circuits and Systems, ICECS 2009*, pp. 1004–1007, Tunisia, December 2009.

[29] M. Bellili, M. Siala, and L. Ben Hadj Slama, "Pulse design for maximizing SIR in partially equalized OFDM/BFDM systems," in *Proceedings of the 2008 IEEE 19th International Symposium on Personal, Indoor and Mobile Radio Communications, PIMRC 2008*, Poland, September 2008.